Atmos. Chem. Phys., 8, 7723–7734, 2008
www.atmos-chem-phys.net/8/7723/2008/

Atmospheric Chemistry and Physics

Tracking and quantifying volcanic SO_2 with IASI, the September 2007 eruption at Jebel at Tair

L. Clarisse[1], P. F. Coheur[1], A. J. Prata[2], D. Hurtmans[1], A. Razavi[1], T. Phulpin[3], J. Hadji-Lazaro[4], and C. Clerbaux[4,1]

[1]Spectroscopie de l'Atmosphère, Service de Chimie Quantique Photophysique, Univ. Libre de Bruxelles, Brussels, Belgium
[2]Norwegian Institute for Air Research, Kjeller, Norway
[3]Centre National d'Etudes Spatiales, 18 Avenue E. Belin, 31401 Toulouse, France
[4]UPMC Université Paris 06, CNRS UMR 7620, Service d'Aéronomie/IPSL, Paris, France

Received: 14 July 2008 – Published in Atmos. Chem. Phys. Discuss.: 9 September 2008
Revised: 27 November 2008 – Accepted: 28 November 2008 – Published: 22 December 2008

Abstract. In this paper we demonstrate the potential of the infrared Fourier transform spectrometer IASI in analysing volcanic eruptions, using the September 2007 eruption at Jebel at Tair as an illustrative example. Detailed radiative transfer calculations are presented, simulating IASI-like transmittance spectra for a variety of volcanic plumes. We analyse the sensitivity of IASI to SO_2 at different altitudes and demonstrate that IASI is in principle capable of sensing SO_2 down to the surface. Using the brightness temperature difference of well chosen SO_2 channels as a filter, we are able to track the plume of the Jebel at Tair eruption for 12 days, on a par with state of the art UV sounders. A method is presented for quickly estimating the altitude of a volcanic plume based on the relative intensities of the SO_2 absorption lines. Despite recent advances, it is still very challenging to retrieve vertical profiles of SO_2 from nadir viewing satellites. Currently the most accurate profiles in nadir are retrieved using backtracking of the plume with atmospheric transport models. Via full inverse retrievals using the optimal estimation method, we show the possibility of extracting medium coarse vertical profiles from IASI data. The retrieval allows us to present an evolution of the total mass of SO_2 in the plume for the Jebel at Tair eruption. An analytical relation is derived between brightness temperature differences and concentrations, which fits the experimental data very well. The spectral range of IASI also allows retrieval of volcanic aerosols. In the initial plume of the Jebel at Tair eruption, volcanic aerosols were found in the form of ice particles, for which we derived particle sizes.

Correspondence to: L. Clarisse
(lclariss@ulb.ac.be)

1 Introduction

Yearly, an estimated 5–20% of the total global sulphur emission is due to volcanic sulphur dioxide (Halmer et al., 2002). The impact of SO_2 on the atmosphere is very much dependent on the height of the eruption. In the troposphere, sulphur dioxide oxidises to sulphate after which it is washed out quickly. The lifetime of SO_2 in the stratosphere is of the order of weeks, during which time it gradually forms sulphuric acid aerosols, which have a lifetime in the atmosphere of about three years. These aerosols have an important impact on the global climate as they increase the earth's albedo through scattering of sunlight. Quantifying natural SO_2 is crucial in comparing natural versus anthropogenic emissions and their respective impact on climate (Andres and Kasgnoc, 1998). Large eruptions also provide an opportunity to validate climate models because of the relatively short perturbation on the climate system (Robock, 2000). Apart from these long term interests, monitoring SO_2 has an application as a surrogate for tracking volcanic ash clouds for aviation hazards (Stunder et al., 2007).

Due to their spatial and temporal distribution, volcanic eruptions are best monitored from space. Traditionally, ultraviolet sounding was mostly utilized for detecting volcanic SO_2, while thermal infrared sounding was traditionally used for the detection of volcanic aerosols. That said, both IR and UV sounders are capable of detecting SO_2, volcanic aerosols (Krotkov et al., 1999; Wen and Rose, 1994) and volcanic ice (Rose et al., 2003). Spaceborne ozone monitors measure radiation using backscattered ultraviolet sunlight (BUV) and are able to measure the SO_2 absorption feature at 230–330 nm. Examples include the Total Ozone Mapping Spectrometer (TOMS, e.g. Krueger et al. (1995)), the Global Ozone Monitoring Experiment (GOME, e.g. Eisinger et al., 1998; Loyola et al., 2008) and more recently the Scanning

Published by Copernicus Publications on behalf of the European Geosciences Union.

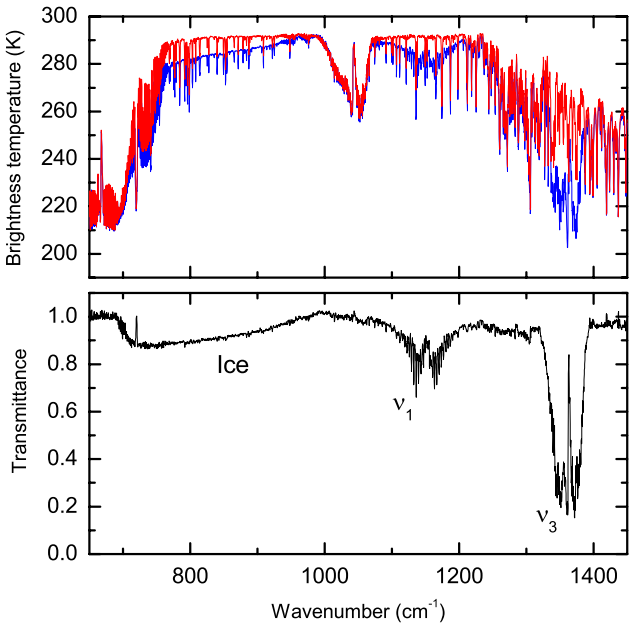

Fig. 1. Top panel. Two spectra (in brightness temperature) from 30 September 2007. The spectrum in blue is taken from inside the initial plume of the Jebel at Tair eruption, the spectrum in red is from a nearby pixel, just outside the plume. Bottom panel. Ratio of the two spectra from the top panel.

Imaging Absorption Spectrometer for Atmospheric CartograpHY (SCIAMACHY, e.g. Lee et al., 2008) and Ozone Monitoring Instrument (OMI, e.g. Yang et al., 2007). Thanks to their large swath these BUV instruments on polar satellites offer a rapid full coverage of the Earth but as they rely on daylight hours, it is only obtained once a day at low latitudes. At high latitudes, depending on the season, it is either not measured, or measured twice or more times a day. Satellite instruments that sound in the infrared do not have this limitation. For the detection of SO_2, they rely on the symmetric stretch ν_1 centred at 1152 cm^{-1}, the antisymmetric stretch ν_3 centred at 1362 cm^{-1} and possibly the weaker $\nu_1+\nu_3$ combination band at 2500 cm^{-1}. Moderate resolution infrared imagers such as the Moderate Resolution Imaging Spectroradiometer (MODIS, e.g. Watson et al., 2004) and the Spinning Enhanced Visible and InfraRed Imager (SEVIRI, e.g. Prata and Kerkmann, 2007) typically have a very good spatial and temporal resolution, but poor spectral resolution. Examples of high resolution IR sounders used to retrieve SO_2 include the Atmospheric Infrared Sounder (AIRS, e.g. Carn et al., 2005), the Tropospheric Emission Spectrometer (TES, e.g. Clerbaux et al., 2008) and the Infrared Atmospheric Sounding Interferometer (IASI).

Recently, the September 2007 eruption of Jebel at Tair was analysed using AIRS, OMI, SEVIRI and lidar backscatter sounder CALIPSO data (Eckhardt et al., 2008). In this paper we demonstrate IASI's potential in analysing volcanic eruptions, using this eruption as an illustrative example.

2 IASI and the eruption on Jebel at Tair

The polar-orbiting MetOp-A was launched on 19 October 2006 and carries on board the Fourier transform spectrometer IASI (see Clerbaux et al., 2007; Phulpin et al., 2007 and http://smsc.cnes.fr/IASI/). It provides global coverage twice a day in the nadir geometry (polar sun-synchronous), with a footprint of 12 km diameter and full swath width of 2200 km. MetOp is an operational platform, so that the measurements are available in near real time. The spectrometer has a spectral coverage from 645 cm^{-1} to 2760 cm^{-1} with no gaps, an apodized resolution of 0.5 cm^{-1} and a spectral sampling of 0.25 cm^{-1}. The instrument covers the ν_1, ν_3 and $\nu_1+\nu_3$ bands of SO_2 completely as well as volcanic ash and aerosol absorption features typical between 800 cm^{-1} and 1300 cm^{-1} (Wen and Rose, 1994). From on-flight analysis the Noise Equivalent Delta Temperature (NEDT) at 280 K is estimated to be 0.05 K in the ν_3 and 0.12 K in the ν_1 band, significantly better than the expected 0.2–0.35 K. These specifications also compare favourably to the AIRS instrument, which has an NEDT of about 0.2 K and only partially covers the ν_1 band (Carn et al., 2005).

Jebel at Tair is a stratovolcano located in the Red Sea between Yemen and Eritrea (15.54° N, 41.83° E), its last eruption dates back to 1883 (see http://www.volcano.si.edu). In the afternoon of 30 September 2007, the volcano violently erupted, killing several people from the Yemen military base on the island. The exact time of the eruption is not known, but it is estimated to have happened between 11:00 and 12:00 UTC (Eckhardt et al., 2008). The first view of the volcanic plume erupted by Jebel at Tair was caught by IASI at 30 September 2007 around 18:48 UTC (Figs. 1 and 8). The plume was tracked for 12 days travelling more than 20 000 km, from Sudan, Egypt, Iraq, Iran, Afghanistan, China, Japan returning through the Philippine Sea, the Philippine Islands, Vietnam, Laos, Myanmar, Bangladesh and finally India (Fig. 2). This compares very well to BUV sounders such as OMI (http://so2.umbc.edu/omi/pix/special/2007/redsea/altair07.php).

3 Altitude information

In this section we outline some spectroscopic features of transmittance spectra relevant to the estimation of the altitude of a volcanic plume. We have simulated radiance spectra for a variety of plumes with different peak altitude and SO_2 concentration, in order to see their impact on the spectra. The calculations were carried out with the software Atmosphit, developed at the Université Libre de Bruxelles (http://home.scarlet.be/dhurtma/atmosphit.html). We start by summarizing the main features of Atmosphit's forward modelling. For the details we refer to Barret et al. (2005a,b), Coheur et al. (2005) and Rodgers (2000).

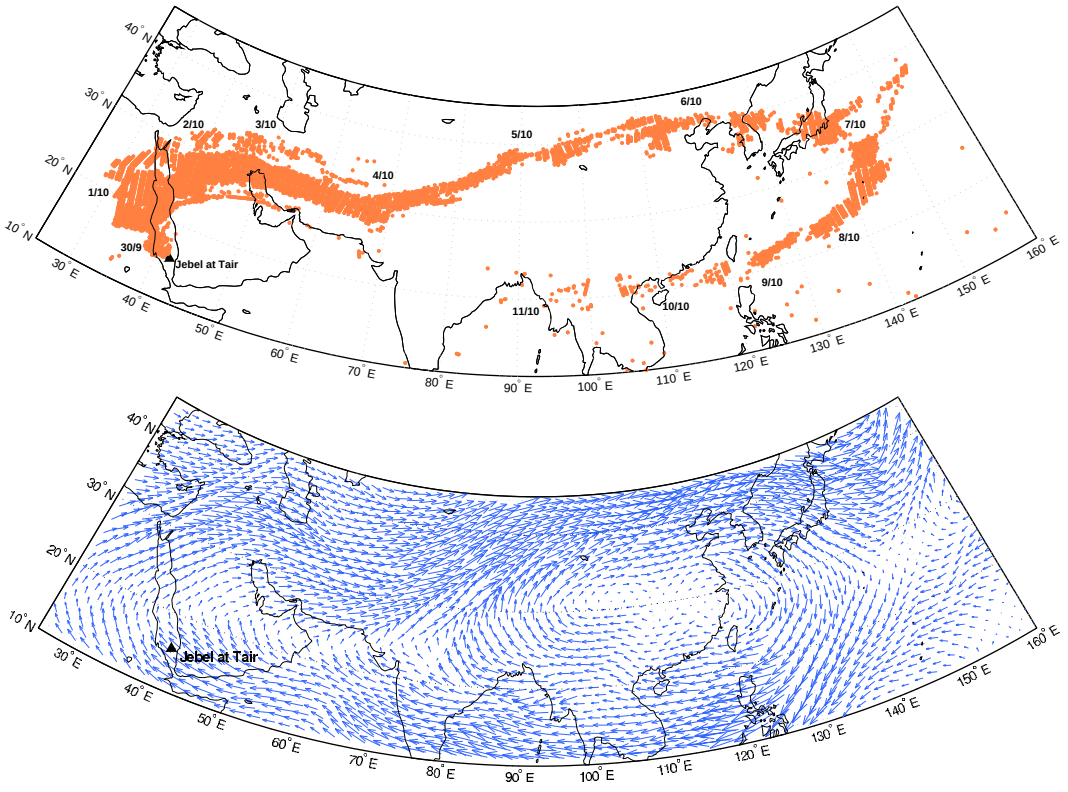

Fig. 2. Top panel. Integrated view (30 September to 11 October 2007) of the SO_2 plume of the Jebel at Tair eruption. The brightness temperature difference in the ν_3 band was used as a tracker (see Sect. 3.2). The coloured dots represent retrieved spectra with a brightness temperature difference larger than 0.5 K. Bottom panel. Wind fields at 100 hPa on 6 October (data from the ECMWF, the European Center for Medium range Weather Forecasting).

3.1 Forward model

Dividing the atmosphere in different layers k, with assumed constant temperature T_k, pressure p_k and volume-mixing ratios, the upward radiance at wavenumber ν entering layer $k+1$ can be approximated by

$$R_{k+1}(\nu) = R_k(\nu)\tau_k + B(\nu, T_k)(1-\tau_k), \quad (1)$$

with τ_k the effective transmittance of layer k and $B(\nu, T)$ the Plank function of a blackbody at temperature T and wavenumber ν. The radiance emitted by the surface is approximated by $R_0{=}\epsilon_s B(\nu, T_s){+}R_r$, with ϵ_s the emissivity of the surface, and R_r the reflected downwelling flux. The first term in Eq. (1) represents the fraction of the radiance entering layer k which is transmitted through layer $k+1$. The second term represents the radiation emitted by layer k. This discrete radiative transfer equation assumes local thermodynamic equilibrium everywhere. To evaluate the radiance emitted at the top of the atmosphere, Eq. (1) is iteratively evaluated for every wavenumber within the range of interest. The effective transmittance is given by

$$\tau_k = \exp\left[-\sum_i \Phi_i(p_k, T_k, n_{i,k}, \nu)C_{i,k}\right], \quad (2)$$

where the sum runs over different species i. Here the coefficients $n_{i,k}$ denote average molecular number densities and $C_{i,k}$ molecular partial columns. In the evaluation of the latter quantity, the effects of refraction are incorporated via ray tracing. The coefficients Φ_i represent the discrete absorption line shape or continuous band shape specific to the species i. These are calculated using a Voigt line shape and the line parameters in the HITRAN database (Rothman et al., 2005). The absorption continua of water vapour, carbon dioxide, oxygen and nitrogen are incorporated using the MT_CKD 1.03 model (Mlawer et al., 2003). Finally the Fourier transform infrared instrumental lineshape of IASI, including apodization and field of view, is taken into account.

3.2 Simulations and discussion

The atmospheric conditions were specified using a standard tropical model (15N latitude) defining average temperature, pressure and volume mixing ratios for 28 molecules in one kilometre thick layers from the ground up to sixty kilometres height. The surface temperature was fixed at 300 K. For each simulation a different amount of SO_2 was inserted in a single 500 m thick layer located between 1 km and 30 km. Figure 3 shows the difference in brightness temperature (BT)

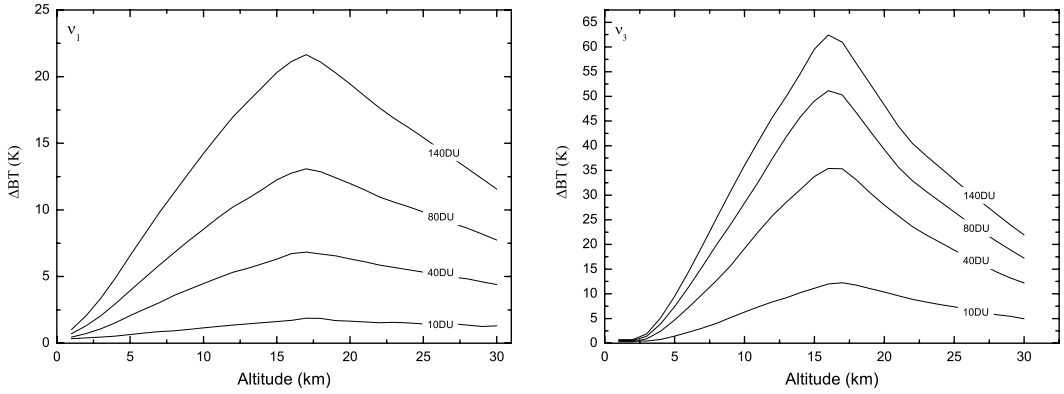

Fig. 3. Brightness temperature differences between the baseline and the average brightness temperature of the three strongest IASI channels of the ν_1 (left) and the ν_3 (right) band as a function of the altitude and concentration of the SO_2 plume.

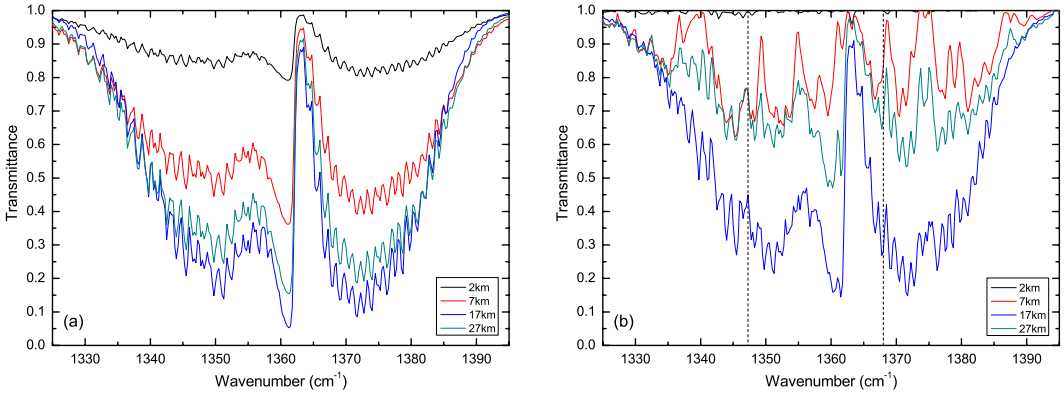

Fig. 4. Simulated IASI-like pseudo transmittance spectra of an atmosphere containing **(a)** only 100 DU SO_2 and **(b)** 100 DU SO_2 and the 28 first HITRAN molecules at a standard tropical concentration.

between the baseline (300 K) and the three strongest absorption lines of the ν_1 and the ν_3 band as a function of the altitude of the SO_2 plume. The specific lines with the strongest absorption vary with altitude and concentration of the plume and give an accurate idea of the sensitivity of IASI. The four different curves represent different amounts of SO_2 in Dobson Units (1 DU equals 2.69×10^{16} molecules per cm^2). Both bands have highest sensitivity between 16 and 18 km, which coincides with the cold point tropopause in the tropical model. The ν_3 band is clearly more sensitive than the ν_1, except below 4 km. In the region 1300–1400 cm^{-1} the water vapour in the atmosphere absorbs nearly all radiation coming from the ground. The atmosphere is only sufficiently transparent at a higher altitude, where the concentration of water vapour is lower (Prata and Bernardo, 2007). For a 100 DU SO_2 plume at 1 km altitude, the highest brightness temperature differences are 1 K in the ν_1 band and 0.7 K in the ν_3 band. IASI has an instrumental noise lower than 0.12 K and should be able to see this. IASI is therefore theoretically capable of sensing volcanic SO_2 in the planetary boundary layer, but much will depend on the precise atmospheric conditions such as the water vapour profile and the thermal contrast between the surface and the first atmospheric layer.

Figure 4 illustrates the impact of water vapour on the observed line intensities. Figure 4a shows the pseudo transmittance spectra of an over-simplified atmosphere containing nothing but 100 DU of SO_2 (again at different altitudes). The only aspect really affecting the intensity of the lines is the thermal contrast between the source (surface) and the temperature of the SO_2 layer. Figure 4b shows the same pseudo transmittance spectra, but this time in an atmosphere populated with water vapour (and the other molecules from the standard model). As mentioned above, water vapour absorbs almost all radiation at low altitude, making the observation almost insensitive to SO_2 in the boundary layer. The spectra in Fig. 4 are pseudo transmittance spectra because they represent the ratio of the BT spectra for an atmosphere with and without SO_2. In contrast, the effective transmittance is only very weakly dependent on the altitude. To scan daily global data for exceptional concentrations of SO_2, we have designed a BT difference filter which calculates BTs at four different IASI channels. The channels at ν_0'=1407.25 and ν_0''=1408.75 are used to estimate the baseline; ν_3'=1371.50 and ν_3''=1371.75 to estimate absorption in the ν_3 band. These

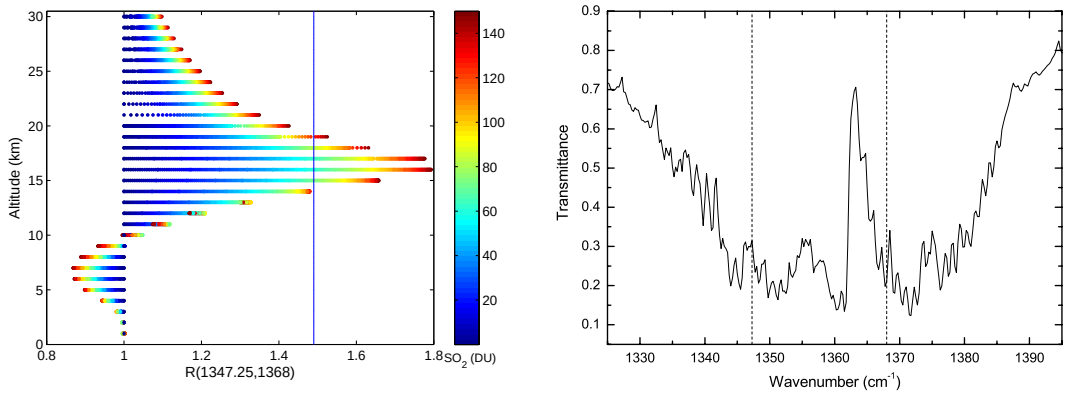

Fig. 5. Intensity ratio $R(1347.25, 1368.00)$ as a function of altitude and concentration. The pseudo transmittance spectrum shown on the right was obtained from an IASI radiance spectrum on 30 September, corresponding to a brightness temperature difference 50 K, divided by a nearby spectrum outside the volcanic plume.

channels were chosen so as to minimise false alerts caused by water vapour interference, while maximising sensitivity. On 30 September, BT differences as large as 50 K (for the ν_3 band) were measured in the plume from Jebel at Tair. In view of Fig. 3 this gives a lower bound of 80 DU on the concentration and puts the peak altitude immediately in the range 12–21 km. For this particular eruption this is already a reasonably good estimate. Absolute intensities for eruptions where the plume does not reach a high altitude will not give us any of this information, as the BT difference will be much smaller.

To quantify the plume's altitude, instead of looking at the absolute intensities, we can also look at the relative intensities of the absorption lines. As an example, Fig. 5 shows the ratio $R(1347.25, 1368.00)$ between the pseudo transmittance coefficients in the IASI channels at 1347.25 cm^{-1} and at 1368.00 cm^{-1} as function of altitude and concentration. For large concentrations of SO_2 this ratio tells us whether the peak altitude is below or above 10 km. For the eruption at Jebel at Tair, typical pseudo transmittance spectra on 30 September have ratios between 1.4 and 1.5, putting the plume in the range 14–19 km with concentrations higher than 60 DU. Analogous results were obtained with other choices of channels for the ratio R. The pseudo transmittance spectra were calculated from the radiance spectra (the target spectra) through division by a reference spectrum. The reference spectra were chosen to have the same baseline as the target spectra without being affected by SO_2. They are typically found geographically close to the target (see also Prata and Bernardo, 2007). It is very important that the reference spectrum is chosen properly, as the ratio R can be quite sensitive to a bad choice. Looking at BT differences and intensity ratios is a quick way of estimating concentration and altitude of a volcanic plume. In the case of large volcanic eruptions, more accurate estimates can be obtained via inverse SO_2 profile retrievals, which we will discuss in detail in the next section.

4 Full retrievals

4.1 Inverse model

As with the forward model, the inverse model was also carried out with the help of Atmosphit. Again, we will sketch the method and refer for details again to Barret et al. (2005a), Barret et al. (2005b), Coheur et al. (2005) and Rodgers (2000). Let us assume for the time being that the forward model is linear, i.e.

$$\boldsymbol{y} = \mathbf{K}\mathbf{x} + \boldsymbol{\epsilon},$$

with $\boldsymbol{y}$ representing the measurement vector (the radiances) and $\mathbf{x}$ representing the state vector (parameters we would like to retrieve such as surface temperature, and concentrations and constant model parameters such as the pressure and temperature profiles). The forward model is represented by the weighting function or kernel $\mathbf{K}$, the measurement error by $\boldsymbol{\epsilon}$.

This type of inverse problem is generally ill-posed, with no exact solution. There are a number of ways to find a regularized solution $\hat{\mathbf{x}}$ which approximates the true state $\mathbf{x}$. The optimal estimation method presented in Rodgers (2000) uses a Bayesian approach. It combines the measurement result $\boldsymbol{y}$ and its measurement covariance matrix $\mathbf{S}_\epsilon$ with the a priori knowledge of the state $\mathbf{x}_a$ and its measured covariance $\mathbf{S}_a$ to yield a maximum a posteriori solution $\hat{\mathbf{x}}$ with covariance $\hat{\mathbf{S}}$. The solution is given by (here we give the so-called n-form of the solution)

$$\hat{\mathbf{x}} = \mathbf{x}_a + (\mathbf{K}^T\mathbf{S}_\epsilon^{-1}\mathbf{K} + \mathbf{S}_a^{-1})^{-1}\mathbf{K}^T\mathbf{S}_\epsilon^{-1}(\boldsymbol{y} - \mathbf{K}\mathbf{x}_a) \quad (3)$$

and

$$\hat{\mathbf{S}}^{-1} = \mathbf{K}^T\mathbf{S}_\epsilon^{-1}\mathbf{K} + \mathbf{S}_a^{-1}.$$

Writing

$$\mathbf{K} = \frac{\partial \mathbf{y}}{\partial \mathbf{x}} \text{ and } \mathbf{G} = \frac{\partial \hat{\mathbf{x}}}{\partial \mathbf{y}},$$

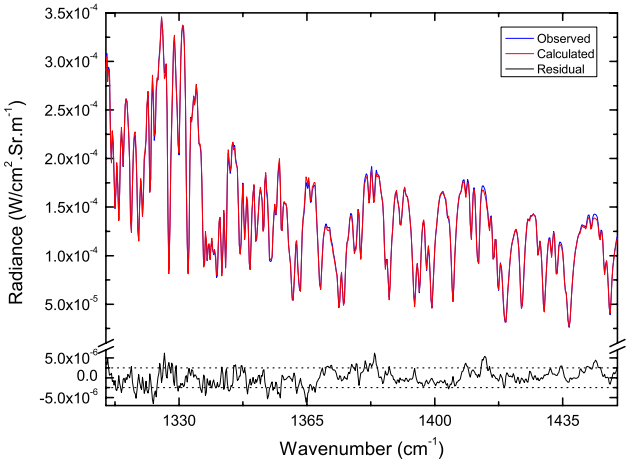

Fig. 6. A sample fit of a spectrum from the first day of the eruption. The dotted lines correspond to $\sigma_\epsilon = \pm 2.5\times10^{-6}$ W/(cm^2·sr·m^{-1}).

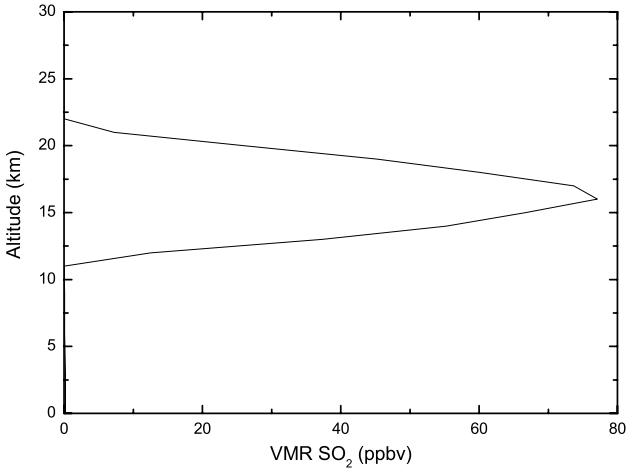

Fig. 7. The retrieved vertical profile of SO_2 corresponding to the spectrum displayed in Fig. 6.

with the gain matrix $\mathbf{G}=(\mathbf{K}^T\mathbf{S}_\epsilon^{-1}\mathbf{K}+\mathbf{S}_a^{-1})^{-1}\mathbf{K}^T\mathbf{S}_\epsilon^{-1}$, we can introduce the averaging kernel

$$\mathbf{A} = \mathbf{GK} = \frac{\partial\hat{\mathbf{x}}}{\partial\mathbf{x}}.$$

In words, the weighting function is the sensitivity of the measurement to the real state, the gain matrix the sensitivity of the retrieved state to the measurement and the averaging kernel the sensitivity of the retrieved state to the true state. In the idealized case where the problem is well determined we have $\hat{\mathbf{x}}=\mathbf{x}+\mathbf{K}^{-1}\boldsymbol{\epsilon}$ and $\mathbf{A}=\mathbf{I}$. More generally though, we can rewrite Eq. (3) as

$$\hat{\mathbf{x}} = \mathbf{Ax} + (\mathbf{I}-\mathbf{A})\mathbf{x}_a + \mathbf{G}\boldsymbol{\epsilon},$$

so that the retrieved state is the weighted average of the true state with the a priori state. The more $\mathbf{A}$ resembles the identity matrix $\mathbf{I}$, the better $\hat{\mathbf{x}}$ will resemble $\mathbf{x}$. The resemblance is commonly quantified by the trace of $\mathbf{A}$ and goes under the name "degrees of freedom for signal" (DFS). It gives an estimate on the number of retrieved independent pieces of information.

For a moderately non-linear problem like ours, we have $\mathbf{y}=\mathbf{F}(\mathbf{x})+\boldsymbol{\epsilon}$. Via Newton methods, the solution can be approximated by the iterative solution

$$\hat{\mathbf{x}}_{i+1} = \mathbf{x}_a + (\mathbf{K}_i^T\mathbf{S}_\epsilon^{-1}\mathbf{K}_i + \mathbf{S}_a^{-1})^{-1}\mathbf{K}_i^T\mathbf{S}_\epsilon^{-1}[\mathbf{y}-\mathbf{F}(\hat{\mathbf{x}}_i)+\mathbf{K}_i(\hat{\mathbf{x}}_i-\mathbf{x}_a)], \quad (4)$$

where $\mathbf{K}=\frac{\partial\mathbf{F}}{\partial\mathbf{x}}$ and $\mathbf{K}_i=\mathbf{K}(\mathbf{x}_i)$.

4.2 Retrieval parameters

For the Jebel at Tair eruption we did not use the ν_1 band for the retrieval. The presence of an ice signature makes an accurate retrieval hard in this band (see Sect. 5). The band is also affected by emissivity features over arid land. The plume passed over both the Arabian desert and the Gobi desert, where the emissivity is strongly dependent on the wavenumber in the region 800–1300 cm^{-1} (see e.g. Li et al., 2007). For the retrievals we considered therefore only the ν_3 absorption feature. The disadvantage of this band is the strong competition of water vapour absorption. An accurate retrieval of the vertical profile of water vapour is essential, and for this reason the fitting range was set to 1310–1450 cm^{-1}. This range not only contains the complete ν_3 band of SO_2, but also contains a large part of the ν_2 band of H_2O. Other interfering molecules in this range include CH_4 and N_2O and total columns were fitted for those. For water vapour, concentrations were retrieved in 1 km thick partial columns, from the surface up to 20 km. For the first 36 h after the eruption, SO_2 was retrieved in three partial columns: 12–15 km, 15–18 km and 18–21 km. This choice was motivated by the analysis presented in Sect. 3. For spectra recorded after 1 October, one total column was fitted between 15–18 km (see Sect. 4.3.2). Apart from the partial and total columns of the different species, the surface temperature has also been fitted. The spectra for the retrieval were selected on the basis of the BT difference between the ν_3 band and the baseline. Only spectra with a BT difference larger than 0.5 K were retained. A priori values for all molecules were taken from either the tropical or midlatitude summer model, and pressure and temperature profiles were interpolated from data from the ECMWF to match date and location of the IASI measurements. The measurement covariance matrix was taken to be diagonal $\mathbf{S}_\epsilon=\sigma_\epsilon^2\mathbf{I}$, with $\sigma_\epsilon=2.5\times10^{-6}$W/(cm^2·sr·m^{-1}), which is of the order of the RMS of a typical spectral fit (see Fig. 6). The a priori covariance matrix $\mathbf{S}_a$ was taken as Gaussian with an off-diagonal coupling constant of 1 km (see Barret et al., 2005a for the explicit formula). For SO_2 the diagonal values of the covariance matrix were chosen proportional to the BT difference in the ν_3 band. For the other molecules they were chosen to

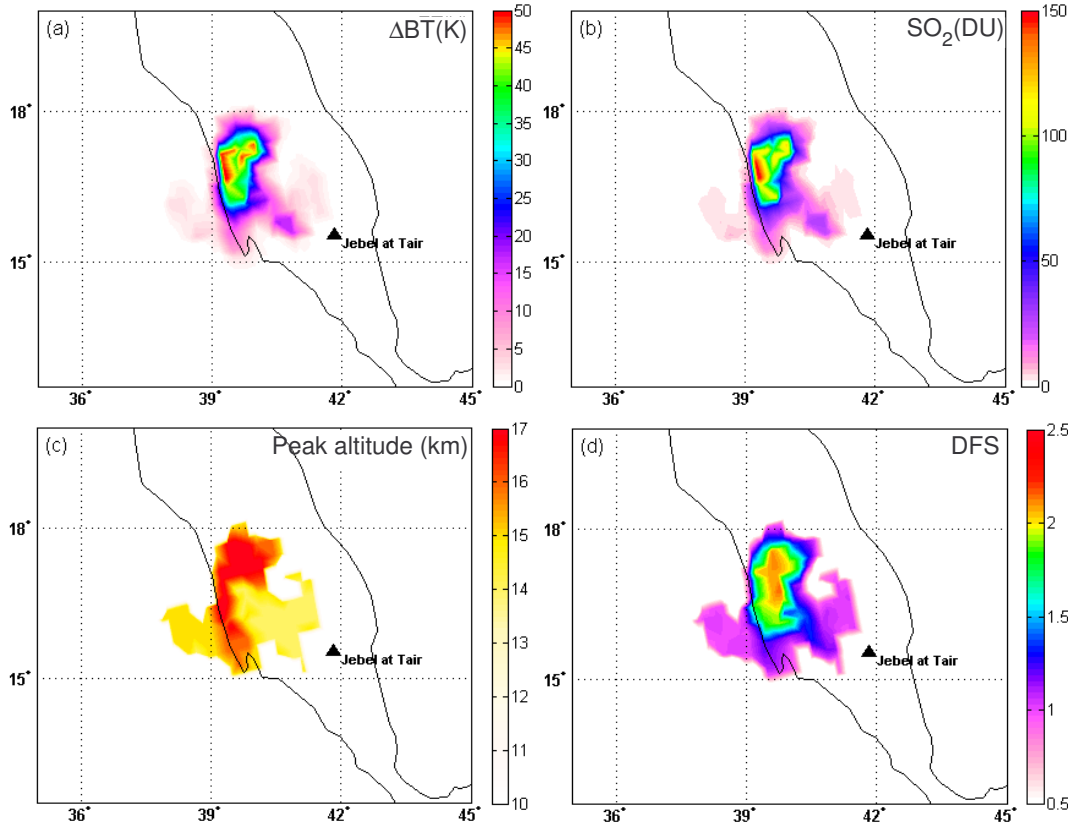

Fig. 8. Different views of the volcanic plume from the eruption at Jebel at Tair on 30 September 2007 around 18:48 UTC. **(a)** Brightness temperature differences in the ν_3 band, **(b)** Retrieved SO_2 concentrations in DU, **(c)** Altitude of peak SO_2 concentration, **(d)** Degrees of freedom for signal.

be constant and corresponding to a relative standard deviation of 25%. The iteration from Eq. (4) was repeated until $|\mathbf{F}(\hat{\mathbf{x}}_i) - \mathbf{F}(\hat{\mathbf{x}}_{i+1})| < 0.2\sigma_\epsilon$.

Note that background values of SO_2 together with a covariance matrix with a very large diagonal and small off-diagonal elements comes close to using a more standard least-squares minimization. An a-priori and covariance matrix could be constructed using the vertical profiles of many different SO_2 plumes. Such information is not available and would remain inadequate viewing the dramatic and unpredictable character of volcanic eruptions. The more general optimal estimation fit was used in this study, as this is the preferred method for the other interfering molecules and gives detailed information on the results (e.g. vertical sensitivity). The choice of taking the a priori variability proportional to the BT difference will be justified in the following section.

4.3 Retrieval of the SO_2 profile

4.3.1 Day of the eruption

A typical fit and corresponding vertical profile for spectra on 30 September are shown in Figs. 6 and 7. Figure 8 summarises the total retrieval, i.e. the brightness temperature difference, the concentration, the DFS of the SO_2 retrieval and the retrieved height of the concentration peak. The first thing to note is the clear correlation between the BT difference and the SO_2 concentration (see in this context also Prata et al., 2003). Figure 9 shows the relation more explicitly. For low concentrations (<30 DU) there is an almost linear correlation between the two, while for higher concentrations the BT difference progressively saturates. This correlation can be derived using simplified versions of Eqs. (1) and (2). Let us assume a layer of SO_2 centred at an altitude of 16.5 km. The radiance at wavenumber ν entering the layer can be written as $B(\nu, T_a)$, where T_a is total brightness temperature of the layers below. The radiance leaving the layer can then be written as

$$B(\nu, T_b) = B(\nu, T_a)\tau + B(\nu, T_{165})(1 - \tau),$$

with T_{165}=192 K the temperature at 16.5 km according to the tropical model, $\tau = \exp(-c_1 C)$ the transmittance, C the SO_2 concentration and c_1 a coefficient dependent on temperature, pressure and thickness of the layer. The BT difference we wish to find is given by $\Delta BT = T_a - T_b$ (in view of the

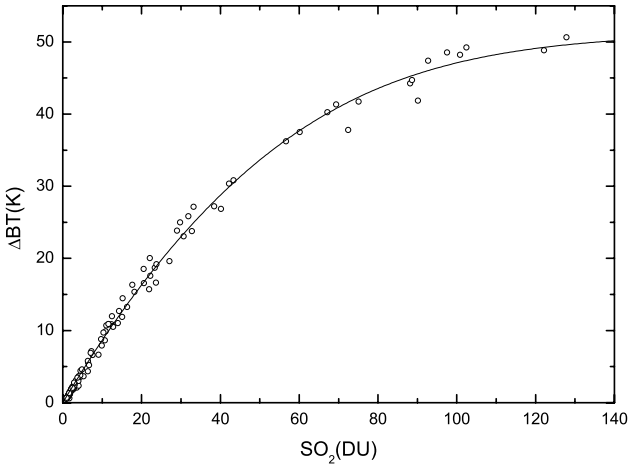

Fig. 9. Correlation between the brightness temperature difference and the retrieved SO_2 concentrations. Each circle represents data from one spectrum, the solid line is given by $\Delta T = T_a - T_b$, with T_b given in Eq. (5) with parameters T_a=243 K and c_1=0.034 DU^{-1}.

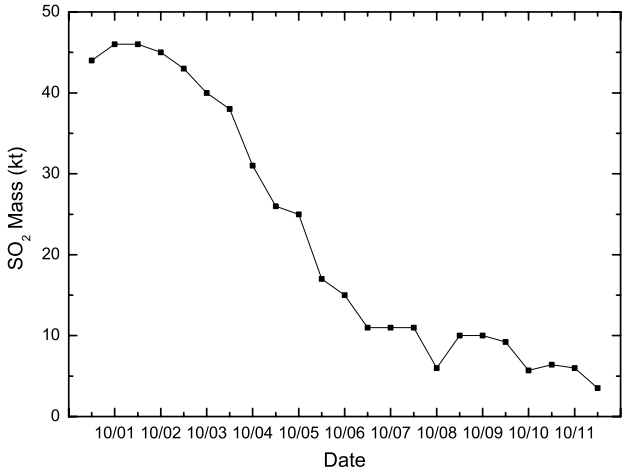

Fig. 10. Evolution of the total mass of SO_2 in function of time. Only retrievals with a RMS smaller than $2\sigma_\epsilon$ were retained for the calculation.

altitude, we ignore absorption above the SO_2 layer). After straightforward calculus one finds

$$T_b = \frac{A}{\ln[1 + GH/(H\tau + G(1-\tau))]}, \quad (5)$$

with $A = hc\nu/k$, $G = \exp(A/T_a) - 1$ and $H = \exp(A/T_{165}) - 1$. From Eq. (5) one can see that when the concentration is very large the observed temperature T_b approaches T_{165}. This again shows the importance of thermal contrasts between T_a and T_b as ΔBT is effectively bounded by $T_a - T_b$. Using linear squares regression, we found values of T_a=243 K and c_1=0.034 DU^{-1}. The resulting curve (Fig. 9) matches the data very well. Note that the a priori variability (covariance matrix) for the SO_2 retrievals was chosen proportional to the BT difference. The non-linear correlation between the concentration and the BT difference indicates that the retrievals were not affected by this choice. We verified on a sample of spectra that – as long as it was chosen large enough, the retrieved concentration is pretty much independent of the variability.

The DFS graph in Fig. 9 shows a moderate correlation with the SO_2 concentration. The maximum DFS is around 2.3; and with a retrieval between 12 and 21 km this corresponds to a vertical resolution smaller than 4 km. It also shows that three partial columns is the right choice for the retrievals for the first day of the eruption. Fewer columns would mean disregarding available information, while more partial columns lead to erratic profiles because of the necessarily large diagonal of the a priori covariance matrix $\mathbf{S}_a$. Another good indication is that for almost all retrieved pixels, the peak of the averaging kernel is the same as the corresponding retrieval level (i.e. the information on a partial column comes primarily from the right altitude). The altitudes where the SO_2 concentration reaches its peak in the profile is typically between 14 km and 17 km. The highest concentrations all had a peak altitude of about 16.5 km. This result is in excellent agreement with information from other satellites and atmospheric transport model simulations (Eckhardt et al., 2008).

4.3.2 Tracking the plume

As shown in Fig. 2, IASI was able to follow the plume for almost twelve days. Three partial columns of SO_2 were fitted from the spectra of the first 36 h after the eruption. Retrievals from spectra after that typically had a DFS of 1 and lower. For this reason, only total columns of SO_2 were retrieved for those. The evolution of the total mass is shown in Fig. 10. It was calculated using the average total column in an area around the observed plume. The first three days after the eruption, the total column peaks around 46 kt, after which it drops to around and below 10 kt. OMI estimated total SO_2 mass (assuming center of mass altitude 17km and 5km thickness) 57kt, 43kt, 31kt and 24kt on October 1 through 4, respectively, which fits well with exponential decay rate 3.4 days (see http://so2.umbc.edu/omi/pix/special/2007/redsea/altair07.php). Figure 10 shows that IASI estimates agree well with OMI tonnages on all days, except on 1 October, when the OMI mass was estimated 25% higher (the OMI overpass was before the beginning of the eruption on 30 September). The reason for disagreement on 1 October needs further investigation.

5 Ice

Ice can be a significant component of volcanic eruption clouds (Rose et al., 2003, 2004) and can hinder retrieval of volcanic ash as well as play a role in scavenging SO_2 (Textor et al., 2003). Ice nucleation may also be a common

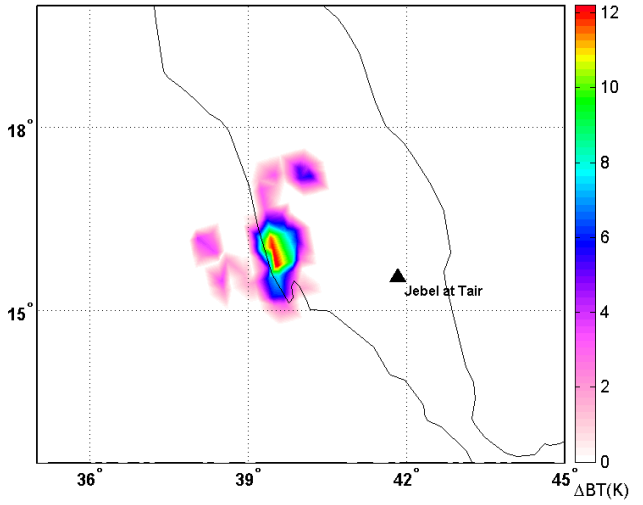

Fig. 11. Brightness temperature difference on 30 September 2007 around 18:48 UTC between the channels at 923.75 cm^{-1} and 996.25 cm^{-1}, indicating the presence of ice.

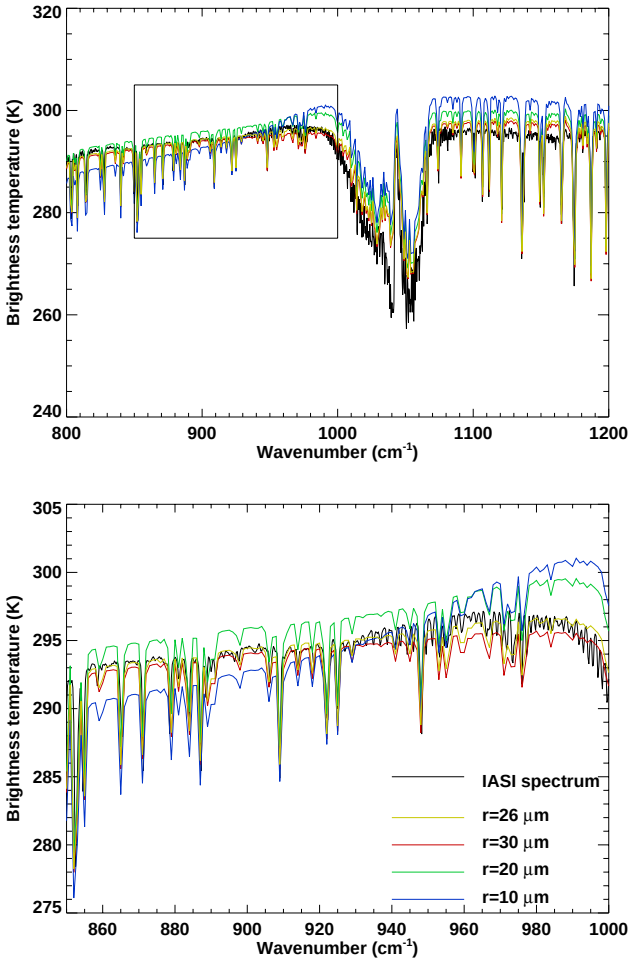

Fig. 12. Top panel. Top-of-atmosphere brightness temperature spectra for an IASI measurements (black) and for simulations using a radiative transfer model with four different mean effective spherical ice particle radii, indicated by different colours. Bottom panel. Close-up of the spectra in the region marked by the box, which includes the atmospheric window within which ice effects are expected to be most pronounced. Notice the change in slope of the BT spectra with wavenumber and the sensitivity of the slope to particle size.

occurrence in volcanic clouds due to the seeding potential of volcanic ash particles (Durant et al., 2008). Measurements from the SEVIRI instrument reported by Eckhardt et al. (2008) suggest that ice was present in the Jebel at Tair eruption cloud. This was deduced by differencing top-of-atmosphere brightness temperatures in SEVIRI channels centred near 11 and 12 μm, which are strongly positive for semi-transparent ice clouds (Wu, 1987). The cause of the differences has been determined through radiative transfer theory (Parol et al., 1991) to be due to differential absorption and scattering by ice (spheres and cylinders have been considered), resulting ultimately from differences in the complex refractive indices of ice at the two wavelengths.

If ice particles were present in the Jebel eruption cloud, then in principle they should be detectable in the IASI brightness temperature spectra, especially within the window region between 800–1000 cm^{-1}. To investigate whether ice was present, we have performed some discrete ordinates radiative transfer calculations for ice spheres using Mie theory, and coupled this with Modtran-4 radiance calculations for atmospheric absorption using a nearby radiosonde profile. The resulting radiances were converted to brightness temperatures and compared directly with an IASI spectrum in the eruption cloud. The real and imaginary parts of the refractive index of ice based on the values provided in Warren (1984) for the region 720–1450 cm^{-1}, tabulated in wavelength (μm) at resolutions of 0.1 to 0.3 μm (10–30 cm^{-1} at 10 μm) were interpolated to the resolution of IASI of 0.25 cm^{-1}. There is a peak in the imaginary part of the refractive index near 800 cm^{-1} and a decrease either side of this maximum. Thus absorption of infrared radiation would be expected to decrease as the wavenumber increases from 800 cm^{-1} to 1000 cm^{-1}. The rate of this decrease in absorption depends on ice particle size and optical depth (Huang et al., 2004). To get an idea of the location of the possible ice plume, we have plotted in Fig. 11 the brightness temperature difference of two almost clear channels at 996.25 cm^{-1} and 923.75 cm^{-1} on 30 September. The location of the ice plume does not exactly coincide with the location of the SO_2 plume, indicating a difference in altitude.

The IASI brightness temperature spectrum of a pixel in the cloud is shown in Fig. 12, together with the radiative transfer simulation. The simulation uses the interpolated refractive indices in a Mie calculation to determine the extinction coefficients due to scattering and absorption, the phase functions and asymmetry parameters for a range of particle sizes

over the wavenumber domain of interest (720–1450 cm^{-1}). These parameters are then used in a discrete ordinates radiative transfer program (e.g. Stamnes and Swanson, 1981) to calculate the brightness temperature spectra for a plane-parallel cloud of varying optical thickness. In this model all radiative processes occurring above the cloud are ignored and the radiances entering the cloud base are calculated from the Modtran-4 radiative transfer program (see Anderson et al., 1995; Berk et al., 1989) with local radiosonde data as input for the temperature and water vapour profiles, while all other gas and aerosol profiles are fixed at the US Standard Atmosphere values. It is noted that there is a potential error in this model, since it is likely that some aerosol (volcanic ash) may be present in the cloud; however in the absence of data on the ash we are unable to include any effects in the model. The brightness temperature spectra for four different mean effective particle radii for an infrared optical depth of 0.30 at 1000 cm^{-1} are shown as coloured lines on Fig. 12. It can be seen that there is a reasonable fit between the simulated spectrum for r=26 μm and the IASI spectrum and poorer fits for the other particle sizes. Of particular interest is the region between 800–1000 cm^{-1} because this region is an atmospheric "window" and likely to show the strongest response to ice, based on the refractive index variation with wavenumber. Thus, when ice is present the slope of the spectrum between 800–1000 cm^{-1} will increase, and will show greatest increase for smallest particle sizes. The IASI spectrum suggests that the ice particles are likely to be at least 20 μm in radius, but not larger than 30 μm. The best fit between the simulations and the IASI spectrum is for a particle radius of 26 μm. The slope appears to be quite sensitive to particle size, a result which agrees with Huang et al. (2004). In particular there is a shoulder in the spectrum within region between 990–1000 cm^{-1} that is especially sensitive and affords the opportunity of determining particle size from high spectral resolution infrared data (e.g. IASI and AIRS). The calculations that have been performed assumed spherical ice particles and it is known that particle shape can alter the phase function and hence influence the radiative transfer. Particle shape has not been investigated here and we refer to prior work (Fu et al., 1999), which suggests that by treating non-spherical ice particles as spheres of equivalent projected area or volume, errors of ~10% may be expected for small particles (r<40 μm) at wavelengths between 8–13 μm. Further research is necessary to investigate whether high resolution infrared spectra can be used to infer ice crystal habit, which may be quite complex in vertically extensive volcanic clouds.

6 Conclusions

The spectral range of IASI covers both the ν_1 and ν_3 band of SO_2 with a good signal to noise ratio. We have analysed IASI's sensitivity to SO_2, and found very good sensitivity for SO_2 at high altitudes and under favourable conditions some sensitivity for SO_2 in the boundary layer. Using the moderate eruption at Jebel at Tair as a test-case, we have demonstrated that the brightness temperature difference of some well chosen channels in the ν_3 band can be used to track SO_2 over a large period and large distance from its source. Depending on concentration, thermal contrast and altitude, also vertical profile information of a volcanic SO_2 plume can be obtained. We have shown here that ratios of relative intensities of absorption lines in the ν_3 band can be used to give estimates of the plume's altitude. Both the tracking of the plume using the brightness temperature filter and the method of estimating the plume's altitude are computationally straightforward. Since the IASI data is available in NRT these methods can be used for operational analysis. We have presented detailed SO_2 profile retrievals using the optimal estimation method, giving us estimates of the concentration and peak altitude. We found that the total SO_2 burden agrees well with OMI measurements. IASI also allows direct detection of volcanic ash and ice and the high spectral resolution allows the retrieval of microphysical properties such as particle sizes. A detailed study of aerosol detection with IASI will be the subject of further research.

Acknowledgements. IASI has been developed and built under the responsibility of the Centre National d'Etudes Spatiales (CNES, France). It is flown onboard the Metop satellites as part of the EUMETSAT Polar System. The IASI L1 data are received through the EUMETCast near real time data distribution service. L. Clarisse and P. F. Coheur are respectively Scientific Research Worker (Collaborateur Scientifique) and Research Associate (Chercheur Qualifié) with F.R.S.-FNRS. C. Clerbaux and J. Hadji-Lazaro are grateful to CNES for scientific collaboration and financial support. The research in Belgium was funded by the F.R.S.-FNRS (M.I.S. n°F.4511.08), the Belgian State Federal Office for Scientific, Technical and Cultural Affairs and the European Space Agency (ESA-Prodex arrangements C90-219). Financial support by the "Actions de Recherche Concertées" (Communauté Française de Belgique) is also acknowledged. The authors would like to thank Jean-Noël Thépaut for providing us with the data of the ECMWF wind fields which were used to produce Fig. 2. The authors are also grateful the anonymous referees and N. Krotkov for their valuable suggestions and corrections.

Edited by: A. Richter

References

Anderson, G., Kneizys, F., Chetwynd, J., Wang, J., Hoke, M., Rothman, L., Kimball, L. M., McClatchey, R., Shettle, E., Clough, S., Gallery, W., Abreu, L., and Selby, J.: FASCODE/MODTRAN/LOWTRAN: Past/Present/Future, 18th Annual Review Conference on Atmospheric Transmission Models, 1–16, 1995.

Andres, R. and Kasgnoc, A.: A time-averaged inventory of subaerial volcanic sulfur emissions, J. Geophys. Res., 103, 25 251–25 261, 1998.

Barret, B., Hurtmans, D., Carleer, M., Mazière, M. D., Mahieu, E., and Coheur, P.-F.: Line narrowing effect on the retrieval of HF and HCL vertical profiles from ground-based FTIR measurements, J. Quant. Spectrosc. Ra., 95, 499–519, 2005a.

Barret, B., Turquety, S., Hurtmans, D., Clerbaux, C., Hadji-Lazaro, J., Bey, I., Auvray, M., and Coheur, P.-F.: Global carbon monoxide vertical distributions from spaceborne high-resolution FTIR nadir measurements, Atmos. Chem. Phys., 5, 2901–2914, 2005, http://www.atmos-chem-phys.net/5/2901/2005/.

Berk, A., Bernstein, L., and Robertson, D.: MODTRAN: a moderate resolution model for LOWTRAN 7., Tech. rep., GL-TR-89-0122, Air Force Geophysics Laboratory, Hanscom AFB., 38 pp., 1989.

Carn, S., Strow, L., de Souza-Machado, S., Edmonds, Y., and Hannon, S.: Quantifying tropospheric volcanic emissions with AIRS: The 2002 eruption of Mt Etna (Italy), Geophys. Res. Lett., 32, L02301, doi:10.1029/2004GL021034, 2005.

Clerbaux, C., Hadji-Lazaro, J., Turquety, S., George, M., Coheur, P.-F., Hurtmans, D., Wespes, C., Herbin, H., Blumstein, D., Tournier, B., and Phulpin, T.: The IASI/MetOp I Mission: First observations and highlights of its potential contribution to GMES, COSPAR Inf. Bul., 2007, 19–24, 2007.

Clerbaux, C., Coheur, P.-F., Clarisse, L., Hadji-Lazaro, J., Hurtmans, D., Turquety, S., Bowman, K., Worden, H., and Carn, S.: Measurements of SO2 profiles in volcanic plumes from the NASA Tropospheric Emission Spectrometer (TES), Geophys. Res. Lett., 35, L22807, doi:10.1029/2008GL035566, 2008.

Coheur, P.-F., Barret, B., Turquety, S., Hurtmans, D., Hadji-Lazaro, J., and Clerbaux, C.: Retrieval and characterization of ozone vertical profiles from a thermal infrared nadir sounder, J. Geophys. Res., 110, D24303, doi:10.1029/2005JD005845, 2005.

Durant, A., Shaw, R., Rose, W., Mi, Y., and Ernst, G.: Ice nucleation and overseeding of ice in volcanic clouds, J. Geophys. Res., 113, D09206, doi:10.1029/2007JD009064, 2008.

Eckhardt, S., Prata, A. J., Seibert, P., Stebel, K., and Stohl, A.: Estimation of the vertical profile of sulfur dioxide injection into the atmosphere by a volcanic eruption using satellite column measurements and inverse transport modeling, Atmos. Chem. Phys., 8, 3881–3897, 2008, http://www.atmos-chem-phys.net/8/3881/2008/.

Eisinger, M. and Burrows, J.: Tropospheric Sulfur Dioxide Observed by the ERS-2 GOME Instrument, Geophys. Res. Lett., 25(22), 4177–4180, 1998.

Fu, Q., Sun, W., and Yang, P.: Modeling of scattering and absorption by nonspherical cirrus ice particles at thermal infrared wavelenghts, J. Atmos. Sci., 56, 2937–2947, 1999.

Halmer, M., Schmincke, H.-U., and Graf, H.-F.: The annual volcanic gas input into the atmoshpere, in particular into the stratosphere: a global data set for the past 100 years, J. Volcanol. Geoth. Res., 115, 511–528, 2002.

Huang, H.-L., Yang, P., Wei, H., Baum, B., Hu, Y., Antonelli, P., and Ackerman, S.: Inference of ice cloud properties from high spectral resolution infrared observations, IEEE T. Geosci. Remote, 42, 842–853, 2004.

Krueger, A., Walter, L., Bhartia, P., Schnetzler, C., Krotkov, N., Sprod, I., and Bluth, G.: Volcanic sulfur dioxide measurements from the Total Ozone Mapping Spectrometer (TOMS) Instruments., J. Geophys. Res., 100, 14 057–14 076, 1995.

Krotkov, N. A., Torres, O., Seftor, C., Krueger, A. J., Kostinski, A., Rose, W., Bluth, G., Schneider, D., and Schaefer, S.: Comparison of TOMS and AVHRR volcanic ash retrievals from the August 1992 eruption of Mt. Spurr, Geophys. Res. Lett., 26(4), 455–458, 1999.

Lee, C., Richter, A., Lee, H., Kim, Y., Burrows, J., Lee, Y., and Choi, B.: Impact of transport of sulfur dioxide from the Asian continent on the air quality over Korea during May 2005, Atmos. Environ., 42, 1461–1475, 2008.

Li, J., Li, J., Weisz, E., and Zhou, D.: Physical retrieval of surface emissivity spectrum from hyperspectral infrared radiances, Geophys. Res. Lett., 34, L16812, doi:10.1029/2007GL030543, 2007.

Loyola, D., van Geffen, J., Valks, P., Erbertseder, T., Roozendael, M. V., Thomas, W., Zimmer, W., and Wißkirchen, K.: Satellite-based detection of volcanic sulphur dioxide from recent eruptions in Central and South America, Adv. Geosci., 14, 35–40, 2008, http://www.adv-geosci.net/14/35/2008/.

Mlawer, E., Clough, S., and Tobin, D.: The MT_CKD water vapor continuum: a revised perspective including collision induced effects, presented at the Atmospheric Science from Space using Fourier Transform Spectrometry (ASSFTS) Workshop, Bad Wildbad, Germany, http://www-imk.fzk.de/asf/ame/ClosedProjects/assfts/O_I_7_Clough_SA.pdf, 2003.

Parol, F., Buriez, J., Brogniez, G., and Fouquart, Y.: Information content of AVHRR channels 4 and 5 with respect to the effective radius of cirrus cloud particles, J. Appl. Meteorol., 30, 973–984, 1991.

Phulpin, T., Blumstein, D., Prel, F., Tournier, B., Prunet, P., and Schlüssel, P.: Applications of IASI on MetOp-A: first results and illustration of potential use for meteorology, climate monitoring, and atmospheric chemistry, Proc. SPIE, 6684, 66840F, doi:10.1117/12.736816, 2007.

Prata, A. and Bernardo, C.: Retrieval of volcanic SO_2 column abundance from Atmospheric Infrared Sounder data, J. Geophys. Res., 112, D20204, doi:10.1029/2006JD007955, 2007.

Prata, A. and Kerkmann, J.: Simultaneous retrieval of volcanic ash and SO_2 using MSG-SEVIRI measurements, Geophys. Res. Lett., 34, L05813, doi:10.1029/2006GL028691, 2007.

Prata, A., Rose, W., Self, S., and O'Brien, D. M.: Global, long-term sulphur dioxide measurements from TOVS data: A new tool for studying explosive volcanism and climate, in: Volcanism and the Earth's Atmosphere, edited by: Robock, A. and Oppenheimer, C., 139, Geophys. Monogr, 75–92, AGU, Washington, D.C., 2003.

Robock, A.: Volcanic eruptions and climate, Rev. Geophys., 38, 191–219, 2000.

Rodgers, C.: Inverse methods for atmospheric sounding: theory and practice, series on athmospheric, oceanic and planetary physics, 2, World Scientific, 240 pp., 2000.

Rose, W. I., Gu., Y., Watson, I. M., et al.: The February–March 2000 eruption of Hekla, Iceland from a satellite perspective, in: Volcanism and the Earth's Atmosphere, edited by: Robock, A. and Oppenheimer, C., 139, Geophys. Monogr, 107–132, AGU, Washington, D.C., 2003.

Rose, W. I., Bluth, G., and Watson, I.: Ice in volcanic clouds: When and where?, in: Proc. of the 2nd Int. Conf. on Volcanic Ash and Aviation Safety, OFCM, Washington, D.C., Session 3, 61, Ex-

tended observations of volcanic SO_2 and sulfate aerosol in the stratosphere, 2004.

Rothman, L., Jacquemart, D., Barbe, A., Benner, D. C., Birk, M., Brown, L., Carleer, M. R., Chackerian Jr., C., Chance, K., Coudert, L., Dana, V., Devi, V., Flaud, J.-M., Gamache, R., Goldman, A., Hartmann, J.-M., Jucks, K., Maki, A., Mandin, J.-Y., Massie, S., Orphal, J., Perrin, A., Rinsland, C., Smith, M., Tennyson, J., Tolchenov, R., Toth, R., Auwera, J. V., Varanasi, P., and Wagner, G.: The HITRAN 2004 molecular spectroscopic database, J. Quant. Spectrosc. Ra., 96, 139–204, 2005.

Stamnes, K. and Swanson, R.: A new look at the discrete ordinate method for radiative transfer calculations in anisotropically scattering atmospheres, J. Atmos. Sci., 38, 387–399, 1981.

Stunder, B. J. B., Heffter, J. L., and Draxler, R. R.: Airborne volcanic ash forecast area reliability, Weather Forecast., 22, 1132–1139, 2007.

Textor, C., H.-F. Graf, H.-F., and Herzog, M.: Injection of gases into the stratosphere by explosive eruptions, J. Geophys. Res., 108, 4606, doi:10.1029/2002JD002987, 2003.

Watson, I., Realmuto, V., Rose, W., Prata, A., Bluth, G., Gu, Y., Bader, C., and Yu, T.: Thermal infrared remote sensing of volcanic emissions using the moderate resolution imaging spectroradiometer, J. Volcanol. Geoth. Res., 135, 75–89, 2004.

Wen, S. and Rose, W. I.: Retrieval of sizes and total mass of particles in volcanic clouds using AVHRR bands 4 and 5, J. Geophys. Res., 99, 5421–5431, 1994.

Wu, M. C.: A method for remote sensing emissivity, fractional cloud cover, and effective cloud temperature of high-level thin clouds, J. Clim. Appl. Meteorol., 26, 225–233, 1987.

Yang, K., Krotkov, N., Krueger, A., Carn, S., Bhartia, P., and Levelt, P.: Retrieval of large volcanic SO_2 columns from the Aura Ozone Monitoring Instrument: Comparison and limitations, J. Geophys. Res., 112, D24S43, doi:10.1029/2007JD008825, 2007.